Spatiotemporal diversity and regionalization of the urban thermal environment in Beijing

QIAO Zhi, TIAN Guangjin

State Key Laboratory of Water Environment Simulation, School of Environment, Beijing Normal University, Beijing 100875, *China*

Abstract: Regionalization of the urban thermal environment is the technical basis for alleviating the conflict between urban socioeconomic development and the thermal environment based on partition management. In this paper, we constructed a regionalization model for the urban thermal environment. (1) Moderate Resolution Imaging Spectroradiometer land surface temperature products from four seasons were standardized and classified for characterizing the spatiotemporal pattern of the urban thermal environment in 2008. (2) A comprehensive evaluation system of the urban thermal environment was constructed and the principal components were identified by using the spatial principal component analysis method. (3) A self-organizing mapping neural network was used for spatial regionalization of the urban thermal environment. The results show that the distribution levels of the urban heat island are clearer during the nighttime than during the daytime and the high-temperature zone has the higher aggregation degree in summer than in the other seasons. The composition of the underlying surface directly affects the urban thermal environment. The principal components affecting the urban thermal environment include vegetation coverage, geomorphology, urban construction scale, and anthropogenic heat emission. The Beijing metropolitan area was divided into seven urban thermal environment zones, and specific measures and suggestions were proposed for improving the urban thermal environment based on the multiple formation mechanisms of the urban thermal environment in each zone.

Key words: thermal environment, regionalization, spatial principal component analysis, artificial neural network, Beijing

CLC number: TP79 **Document code:** A

Citation format: Qiao Z and Tian G J. 2014. Spatiotemporal diversity and regionalization of the urban thermal environment in Beijing. Journal of Remote Sensing, 18(3): 715 - 734 [DOI: 10.11834/jrs.20143030]

1 INTRODUCTION

Urban development will dramatically change the underlying surface and atmospheric properties. The changes in surface albedo, temperature, humidity, and aerodynamics will induce a series of microscale and medium-scale climate changes (Roth, et al., 1989). Urban Heat Island (UHI), which is defined as urban temperature being higher than in suburbs (Oke, 1982), is inevitable during urban development. From the perspective of spatial structure, UHI is composed of multiple timescales and multiple centers. The UHI is superimposed on several heat islands at various scales (Jiang, et al., 2004). From the perspective of temporal change, UHI intensity significantly changes daily and seasonally, with maximum change in the daytime and warm season (Schmidlin, 1989). UHI intensity decreases with increased wind speed or cloud cover (Kidder & Essenwanger, 1995), but increases at higher urban population scale (Yamashita & Sekine, 1990). The influence sphere of the UHI Effect (UHIE) is expanding globally, which will severely affect regional climate, urban atmospheric environment, energy consumption, and human health. The UHI-caused high-temperature disasters will bring huge economic losses. UHI circulation will enhance suburban convection and bring more frequent floods. UHI will degrade environmental quality and make pollutants hard to diffuse, which will trigger urban diseases. Recently, "urban diseases" have become increasingly serious. The high temperature and heat wave in summer and the large-scale dust-haze induced by deteriorated urban ventilation in winter will severely harm human health and quality of life. Therefore, healthy and science-based urbanization has become the key and state-level requirement, because it concerns China's rapid and positive socioeconomic development and the improvement of quality of life.

At the beginning, air temperature data were used in monitoring and research on UHIs. The "UHI" was actually Atmospheric Urban Heat Island (AUHI), which is divided into urban boundary layer heat island and urban Canopy Layer Heat

Received: 2013-02-05; **Accepted:** 2013-11-05; **Version of record first published:** 2013-11-12

Foundation: National Natural Science Foundation of China (No. 41071357); National Key Technology Research and Development Program of China during the Twelfth Five-Year Plan Period (No. 2012BAC13B01)

First author biography: QIAO Zhi (1986—), male, Ph. D. candidate, he majors in GIS and remote sensing of environment. E-mail: george@mail.bnu.edu.cn

Corresponding author biography: TIAN Guangjin (1970—), male, Ph. D. candidate, associate professor. His research interests are urban dynamic model, remote sensing of environment, GIS, and land use cover/change. E-mail: tianguangjin@bnu.edu.cn

Island (CLHI). In AUHI, the data measured by a fixed or mobile thermal detector in direct contact with air are used to represent the difference in atmospheric temperature between the urban area and the suburban area. Thereby, the obtained data are discrete or linear data. Considering continuity in time, AUHI can be used for day-night, between-month, between-year, or present-history comparison. Rao (1972) introduced thermal infrared Remote Sensing (RS) into study on UHI, signifying a new stage in this field, namely, the temperature data reversed from thermal infrared RS data are used as Land Surface Temperature (LST) to represent Surface Urban Heat Island (SUHI) (Voogt & Oke, 2003; Chen, et al., 2012). Thermal infrared RS data cover large areas and have high spatial resolution and continuity. With the development of RS, the temporal resolution of thermal infrared RS data has also been significantly improved. The LST data inverted from thermal infrared RS have higher spatiotemporal diversity, higher correlation with land use types, and higher UHI intensity than AHUI and, thus, are more sensitive to land surface changes and human activities (Roth, et al., 1989; Voogt & Oke, 2003).

The study of regionalization aims to investigate the formation of regional units, space-time differentiation, and regulating measures and, thus, to maximize the benefits in regional development (Zheng, et al., 2005). With the rapidly increased urban population and urbanization, unreasonable urban planning will aggravate urban thermal environment, while the inevitable trend of compacted and high-density cities will raise the requirements for urban environment protection. However, at the current stage, identification and improvement of the urban thermal environment through regionalization are lagging far behind. Under the same weather condition, the urban thermal environment is related to urban scale and distribution, population density, building density, vegetation coverage, land use, and urban underlying surface. Therefore, the regionalization scheme suitable for one city cannot be fully copied by another city. Properly understanding the relationship between different factors in urban underlying surface and the thermal environment is the key to deepen urban thermal environment studies. Even the seasonal or day-night contributions of underlying surface types to regional thermal environment are different (Qiao, et al., 2013). The driving factors on urban thermal environment will be analyzed to investigate the forming mechanism of UHI, build urban thermal environment regionalization schemes, and guide the regulation and prevention of the main factors causing the urban thermal environment. Therefore, we can finally propose the methods to improve the urban thermal environment and alleviate or control UHI. In this paper, MODIS LST products were used to analyze the spatiotemporal patterns of LST in Beijing. We further build a thermal environment influence factor assessment system for Beijing. Finally, Spatial Principal Component Analysis (SPCA) and Self-Organizing Mapping (SOM) neural network were used in the regionalization of the urban thermal environment in Beijing. This study provides some references for urban planning and urban ecological risk assessment.

2 STUDY AREA

Beijing is located in the north part of the North China Plain. The altitude is high in the northwest and low in the southeast. Beijing extends to the Yanshan Mountains in the north, to the Taihang Mountains in the west. The city has a subhumid warm temperate continental monsoon climate and four distinct seasons, with a cold and windy winter and a hot and humid summer. Beijing has an annual average temperature of 10—12℃ and an annual rainfall of 600—700 mm. In the past 50 years, the population of Beijing has increased by 6.5 times, the investment into infrastructure has increased by nearly 390 times, and the area of housing has increased by 40 times (Zhang, et al., 2011). The e xpanding urban scale and the increasing urbanization in Beijing will severely affect the urban thermal environment. Other studies show that the UHI intensity increases by 0.043℃ with the i ncrease of 10^6 m^2 of building area and by 0.16℃ with the i ncrease of 10 billion Yuan in infrastructure investment. The LST decreases by 1.6℃ with the increase of 0.1 of Normalized Difference Vegetation Index (NDVI) (Lin, et al., 2005).

3 DATA SOURCES

MODIS is a crucial instrument aboard National Aeronautics and Space Administration's Terra (formerly, Earth Observing System [EOS] AM) and Aqua (EOS PM) satellites for global studies of atmosphere, land, and ocean processes. Terra was launched on December 18, 1999, and its overpass times are a round 1030 (local solar time) in its descending mode and 2230 local solar time in its ascending mode. The MODIS LST products have been extensively used in investigations of the U HIE. The split window algorithm is used to retrieve LST by applying multiple bands from the thermal and middle infrared spectral bands of MODIS. The spatial resolution is 1 km. The a ccuracy of the products has been verified to be approximately 1 K of the root-mean-square error (Wan, et al., 2004; Wang, e t al., 2007; Wang, et al., 2007). The MODIS bidirectional r eflectance distribution function/albedo products are used to r etrieve the NDVI and Normalized Difference Buildup Index (NDBI).

To retrieve the land cover types, Landsat TM images were chosen and radiantly corrected. The images were false color composed of five, four, and three bands using the red-green-blue method of artificial visual interpretation. The six aggregated classes of land use are: cropland, forest, grassland, water bodies, built-up land, and bare land. These classes were further divided into 25 land use classes. The built-up land contains urban land, rural residential land, and industrial and mining sites (Liu, et al., 2005). The land use dataset was provided by the Institute of G eographical Sciences and Natural Resources Research, C hinese A cademy of Sciences (CAS). In addition, the digital city data of Beijing metropolitan area is used in the study. The dataset includes the vector data of administrative boundary, water bodies, parks, railways, roads, and blocks (Tian, et al., 2010).

4 METHODS

4.1 Processing of MODIS LST data

The MODIS LST products first underwent batched geometric correction on the MODIS Reprojection Tool and then were

masked by the Beijing metropolitan area and resampled to pixels of 1000 m × 1000 m. The head files of the MODIS LST products show that the radiation scaling ratio is 0.02 and the r adiation scaling distance is 0. The LST (℃) for Beijing is calculated as Eq. (1).

$$T_s = \mathrm{DN} \times 0.02 - 273.15 \quad (1)$$

where T_s is the LST and DN is the pixel gray value. Given that the DN of MODIS LST products in cloud-covered areas is 0, the temperature in these areas is calculated to be −273.15℃, and thus, cloud mask is necessary to remove the outlier. These procedures were conducted on the Arc/Info workstation.

4.2 Spatiotemporal distributions of LST

To avoid the effects of clouds, eight high-quality images on April 22, July 19, October 7, and December 2, 2008 were selected to be representative of spring, summer, autumn, and winter, respectively. To characterize the spatial distribution of LST at different seasons, LSTs were normalized and then the u rban thermal environment was classified by using the density segmentation method (Jiang & Qiao, 2012). First, LSTs at different seasons were normalized between 0 and 1.

$$T_{ni} = \frac{T_{si} - T_{\mathrm{smin}}}{T_{\mathrm{smax}} - T_{\mathrm{smin}}} \quad (2)$$

where T_{ni} is the normalized value of the pixel i, T_{si} is the LST of the pixel i, T_{smax} is the maximum LST in Beijing, and T_{smin} is the minimum LST. Then, the normalized LSTs were classified by density s egmentation method into seven thermodynamic levels: very low, low, sub-medium, medium, sub-high, high, and ultrahigh (Table 1). Thereby, the distribution characteristics of the LST level in Beijing were obtained, and the area of each level could be calculated. In this paper, the Aggregation Index (AI) was used to r epresent the spatiotemporal diversity of LST level in Beijing. The AI is calculated on basis of the common boundary between the same levels of pixels. For one level, when the common boundary of all pixels is the longest, the AI is maximal, indicating that this level of pixels is most aggregated and c oncentrated.

Table 1 LST classification criteria

LST level	LST range
Very low	$T_{ni} < T_{\mathrm{mean}} - 2.5s$
Low	$T_{\mathrm{mean}} - 2.5s \leqslant T_{ni} < T_{\mathrm{mean}} - 1.5s$
Sub – medium	$T_{\mathrm{mean}} - 1.5s \leqslant T_{ni} < T_{\mathrm{mean}} - 0.5s$
Medium	$T_{\mathrm{mean}} - 0.5s \leqslant T_{ni} < T_{\mathrm{mean}} + 0.5s$
Sub – high	$T_{\mathrm{mean}} + 0.5s \leqslant T_{ni} < T_{\mathrm{mean}} + 1.5s$
High	$T_{\mathrm{mean}} + 1.5s \leqslant T_{ni} < T_{\mathrm{mean}} + 2.5s$
Ultrahigh	$T_{ni} \geqslant T_{\mathrm{mean}} + 2.5s$

Note: T_{ni} is the normalized value of a pixel, T_{mean} is the mean of all pixels after normalization, and s is standard deviation.

4.3 The assessment system of the urban thermal e nvironment

The formation and evolution of the urban thermal environment directly relate to the quality and sustainable development of the urban ecological environment (Yue, 2008). For a metropolitan area as a complex macrosystem, the urban thermal environment is affected by various factors, including thermal i nertia, heat capacity, heat conduction, thermal radiation of the underlying surface, human activity intensity, distribution of landscapes, and internal structure. RS and survey data were used to build an assessment system for comprehensive multivariable a nalysis of the urban thermal environment and for r evealing the forming mechanism of the urban thermal environment.

The assessment systems of the urban thermal environment index have been built for Shanghai, Beijing-Tianjin-Hebei M etropolitan Circle, and southeast Fujian city group (Yue, 2008; Meng, et al., 2010; Yu, 2011). Two factors will induce UHI: the difference in land use types and covers between the urban and the suburban areas and the difference in gas and heat emissions from traffic, production, and life between urban and suburban a reas (Chen, et al., 2012). Throughout the processing of urban development, the UHIE-promoting factors have been strengthened, while the UHIE-alleviating factors have been weakened. In the assessment system of the urban thermal environment influence index, therefore, land use types and anthropogenic heat emissions should be combined to highlight their effects on local climate and, thereby, to propose more specific thermal environment regulating measures. In this paper, the social, economic, and natural conditions were combined to build the assessment systems of the urban thermal environment index for Beijing (Table 2).

Table 2 The assessment systems of the urban thermal environment index for Beijing

	First-level index		
	Urban underlying surface	Human activity	Ecological environment
Second-level index	NDBI	Road density	Elevation
	SHDI	Population density	Slope
			NDVI

The assessment systems of the urban thermal environment index for Beijing can be divided into two levels: the first level concerns the characteristics of urban underlying surface, the characteristics of human activity, and the characteristics of e cological environment. Each first-level index can be divided into several second-level indices. Human activity intensity includes the heat released from production and life, but can be hardly quantified directly from RS data. In this paper, road density and population density are used as indices reflecting a nthropogenic emissions (e. g., vehicle exhaust, refrigeration and heating emissions). The connotations and calculation methods of second-level indices are explained below.

NDBI accurately reflects the information of construction land (Zha, et al., 2003). A larger NDBI indicates higher proportion of building land and higher building density. In this paper, NDBI is used to represent the spatial distribution of urban impervious surface, calculated as Eq. (3).

$$\mathrm{NDBI} = \frac{Q_{\mathrm{SWIR}} - Q_{\mathrm{NIR}}}{Q_{\mathrm{SWIR}} + Q_{\mathrm{NIR}}} \quad (3)$$

where Q_{SWIR} is the gray level of shortwave infrared band and Q_{NIR} is the gray level of near-infrared band, corresponding to the sixth and second bands for MODIS surface reflectivity products, respectively. Using the MODIS data in Changsha-Zhuzhou-Xiangtan area (within -0.411 to 0.061), Li, et al. (2009) observed no obvious change for NDBI in the four seasons, indicating that NDBI will not change largely with seasons.

Shannon's Diversity Index (SHDI) based on information theory is a comprehensive reflection of the richness and complexity of landscape patterns (Yue, 2008). Urban LST is closely related to landscape types in the underlying surface and to spatial combination of landscape types. The SHDI of the urban underlying surface is in quadratic parabola relationship with the landscape-related heterogeneity of LST (Wang, et al., 2012). The SHDI is calculated as Eq. (4).

$$\mathrm{SHDI} = -\sum_{i=1}^{m}(P_i \times \ln P_i) \quad (4)$$

where P_i is the proportion of area of land use i and m is the number of this land use type. The present land use map was overlain with 1 km × 1 km fishnet in the study area to summarize the proportions of different land use types in each fishnet and to calculate the SHDI.

Road density is based on road levels as measuring standard, and the weights are assigned based on road levels. Road density is calculated by the linear density function in Arc/Info as Eq. (5) (Yue, 2008).

$$R_{\mathrm{d}} = \frac{((L_1 \times W_1) + (L_2 \times W_2) + \cdots + (L_n \times W_n))}{Area} \quad (5)$$

where R_{d} is the road density, L_n is the road length in a 1 km × 1 km fishnet, W_n is the road weight, and $Area$ is the pixel area.

Population density is the ratio of population in the area at a certain period and reflects the geographical denseness of population. The 1 km resolution ratio of the population statistics dataset was provided by the CAS. This dataset was obtained by using demographic spatialization technology, selecting urban area, rural residential area, and cropland that most relate to population spatial distribution, and by building a demographic spatialization model of statistics data with towns as example (Yang, et al., 2006).

Considerable research has confirmed that LST is inversely proportional to elevation and slope because a low elevation and a small slope are contributive to the formation of heat island center (Zhang, et al., 2007). The digital elevation model used in this paper is masked by the administrative region of Beijing for calculation of slope by Arc/Info software.

NDVI reflects the relative abundance and active radiation amount of vegetations and indicates the difference in surface properties between urban land and rural areas (evaporation and heat capacity). However, NDVI cannot clearly reflect the surface properties in winter because Beijing is dominated by deciduous vegetation, which has weak photosynthetic activity in winter.

$$\mathrm{NDVI} = \frac{Q_{\mathrm{NIR}} - Q_{\mathrm{Red}}}{Q_{\mathrm{NIR}} + Q_{\mathrm{Red}}} \quad (6)$$

where NDVI is the normalized difference vegetation index, Q_{NIR} is the gray level of near-infrared band, and Q_{Red} is the gray level of red band, corresponding to the second and first bands for MODIS surface reflectivity products, respectively.

Given that the influence factors have different grading or units, their effects on the urban thermal environment cannot be compared and must be quantified. Therefore, the factors were normalized by range standardization.

$$X_i' = \frac{X_i - X_{\min}}{X_{\max} - X_{\min}} \quad (7)$$

where X_i' is the normalized value of an influence factor, X_i is the original value, and $X_{\min}$ and $X_{\max}$ are the minimum and maximum of the influence factor throughout the study area, respectively. Through normalization, the effects of range and dimension could be eliminated.

4.4 SPCA of urban thermal environment influence factors

The urban thermal environment is under the influence of many factors, and a certain correlation can be observed between these factors. As such, direct multicriteria diagnosis is impossible (Yue, 2008). Therefore, orthogonal rotation transform in SPCA is used to eliminate the correlation or redundancy among these factors, and thereby, the physical meaning of each principal component can be defined, avoiding the disadvantages in multicriteria weight judgment and further revealing the internal mechanism of the urban thermal environment. With the support of GRID function on Arc/Info, the SPCA is used to investigate the formation of the urban thermal environment. Principal components were selected through calculation of eigenvalues and contribution rates for targeted spatial factors related to the urban thermal environment in Beijing. The physical significance of each principal component for the formation of the urban thermal environment is defined to further reveal the forming mechanism of UHI.

4.5 The regionalization of the urban thermal environment based on SOM

On the Self-organizing Feature Map (SOM) neural network model, the inputted variables experience unsupervised clustering by seeking the optimal weight vector. This method avoids subjectivity which is encountered in artificial determination of weight for each index or each level. The SOM model will be increasingly used in the simulation of urban systems (Ling & Xu, 2003; Yue, 2008; Hao, et al., 2008). Geographic Information System (GIS) and SOM were combined spatially to simulate competition among spatial samples and to perform spatial clustering, thereby improving the application ability of SOM and providing a new method for planning and dividing the urban thermal environment.

The SOM network is composed of an input layer (to receive input modes) and a competition layer (in which neurons are arranged in two-dimensional arrays). The neurons between the two layers are two-way connected. The SOM network clusters and simulates the inputted modes by seeking the optimal weight vector (Ling & Xu, 2003).

The input mode of the network is $P_k = (p_1^k, p_2^k, \cdots, p_N^k)$, $k = 1, 2, \cdots, q$. The neuron vector in the competition layer is $A_j =$

$(a_{j1}, a_{j2}, \cdots, a_{jM})$, $j = 1, 2, \cdots, M$, where P_k is a continuous value, A_j is a digital amount, q is the number of learning modes, N is the number of neurons in the input layer; and M is the number of neurons in the competition layer. The connection weight vector between the neuron j from the competition layer and the neuron from the input layer is

$$W_j = (w_{j1}, w_{j2}, \cdots, w_{jN}), j = 1, 2, \cdots, M$$

The principal components from SPCA were inputted into SOM. With the support of MATLAB and GIS, the forming mechanisms of the urban thermal environment in Beijing are spatially clustered to reveal their spatial difference, summarize their main types, regionalize the thermal environment in Beijing, and propose measures for relieving UHI.

5 RESULTS

5.1 Spatiotemporal distributions of the urban thermal environment

Among all levels of temperature zones, the medium-temperature zones occupy the largest proportion. Based on the meanings of temperature levels, the medium-temperature zone can be regarded as the "mean" LST in Beijing at a certain period. Therefore, the spatiotemporal diversity of LST in Beijing can be more significantly represented by anomaly analysis of "low-temperature zones" (including low, sub-low, and sub-m edium) and "high-temperature zones" (including sub-high, high, and ultrahigh) (Fig. 1 and Table 3).

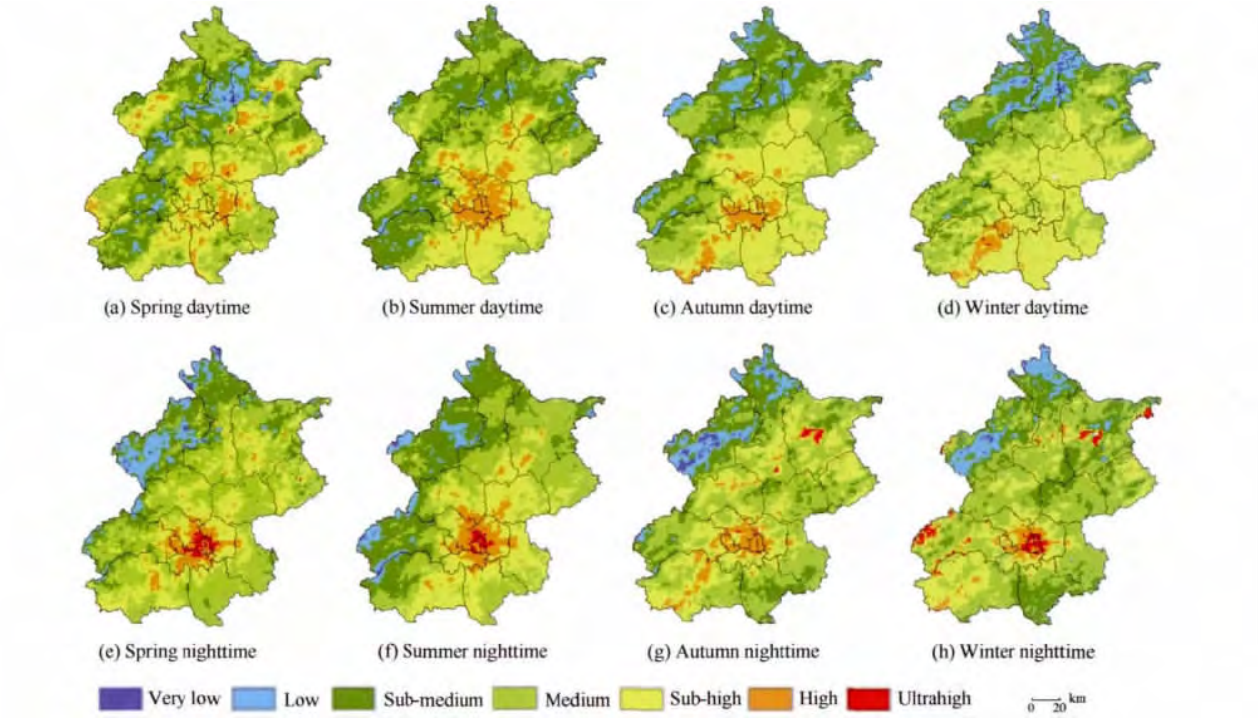

Fig. 1 Spatiotemporal distribution of LST levels in Beijing in 2008

Table 3 Proportions of LST levels in Beijing in 2008

Levels	Daytime				Nighttime			
	Spring	Summer	Autumn	Winter	Spring	Summer	Autumn	Winter
Very low	0.24	0.01	0.01	0.79	0.62	0.29	1.23	0.38
Low	6.92	3.80	7.45	8.70	7.97	5.64	6.07	5.71
Sub-medium	24.54	34.22	25.80	20.03	18.01	26.61	20.13	22.55
Medium	34.79	27.95	29.83	30.42	42.58	34.68	41.16	44.28
Sub-high	27.07	25.60	31.25	37.21	24.55	25.47	24.93	20.00
High	6.34	8.42	5.66	2.81	5.29	6.59	6.03	5.08
Ultrahigh	0.10	0.00	0.00	0.04	0.99	0.72	0.45	2.00

In analysis of temperature level distributions at daytime and nighttime, the medium-temperature zones account for a larger proportion at nighttime than at daytime, while "low-temperature zones" and "high-temperature zones" account for smaller proportions than at daytime, indicating that nighttime temperature in Beijing is less spatially different than at daytime. Regarding spatial distribution, the aggregation indices of nighttime temperature levels are higher than at daytime and nighttime UHI distribution is more hierarchical or, namely, the high-temperature zones extend from the city center through the sub-high-temperature zones in the suburb to the low-temperature zones in the periphery. Such distribution is due to the urban-rural differences in surface absorption and heat storage performance. With small solar reflectivity, large thermal capacity, and high thermal conductivity, the urban underlying surface stores more heat. The surface longwave radiation reflects several times between buildings and ground surface. Hence, surface longwave radiation radiates less energy to the air. However, compared with

daytime, the ultrahigh-temperature zones at nighttime are distributed in two different ways: (1) They concentrate in the urban area and are apparent in spring, summer, and fall, but not in winter, probably because of the intense urban human activity and concentrated heat supply and cooling. (2) They concentrate in large-area water bodies, such as Miyun Reservoir, because of the large specific heat of water and small temperature variation under cooling or heating conditions.

Analysis of seasonal temperature change shows that, in summer, medium-temperature zones at daytime account for the smallest proportion, followed by "high-temperature zones," but "low-temperature zones" occupy a large proportion. These changes are different at daytime in winter. Regarding the AI, the "high-temperature zones" at daytime in summer account for the largest proportion, centered in the urban area and radiating outward, indicating a high UHI intensity (Table 4). The inland urban temperature at daytime is highly correlated with land use types, as it is the highest in industrial land use, but lowest in vegetation and rivers. Terra passes Beijing at 10:30, when LST is rising. The suburbs in Beijing are covered by mountains and the vegetations are dense in summer. As such, temperature is far lower than in the urban area. However, the vegetations in Beijing are dominated by deciduous vegetation. As such, the withering-exposed surface in winter, frozen soil, and stronger radiation cooling make the temperature difference smaller than in summer and "low-temperature zones" are not apparent. The AI of "high-temperature zones" at winter daytime is very low and scattered, indicating the strong effect of human activities. In particular, large-area high-temperature zones appear in the middle and north parts of Fangshan District, where industrial enterprises with low energy efficiency are spread. In addition, in winter daytime, an "urban cold island" appears in Beijing.

Table 4 AI of LST levels in Beijing in 2008

Levels	Daytime				Nighttime			
	Spring	Summer	Autumn	Winter	Spring	Summer	Autumn	Winter
Very low	58.46	N/A	N/A	45.15	54.10	57.32	66.76	46.36
Low	71.95	60.72	68.63	68.15	71.15	75.10	72.69	78.04
Sub-medium	73.36	83.39	79.75	73.09	71.70	86.67	75.16	75.19
Medium	74.04	77.31	82.02	72.97	80.48	84.25	81.15	80.04
Sub-high	76.81	84.16	89.20	83.86	75.36	83.85	78.10	72.13
High	66.96	81.27	78.97	73.32	72.21	83.14	74.91	62.89
Ultrahigh	37.50	0.00	0.00	57.14	71.81	78.50	76.92	68.40

5.2 SPCA of urban thermal environment influence factors

The previously presented analysis shows that the high-temperature zones and low-temperature zones have the characteristics of centralized distribution in Beijing in summer daytime, indicating that the influenced area of heat island is larger. The dense vegetation in summer is more effective in reducing urban temperature than in winter. In addition, human activity intensity at daytime is also higher than at nighttime. Therefore, we selected the factors inputted to PCA related to summer daytime LST, which best represents the thermal environment in Beijing. Thereby, the contributions of all factors to the thermal environment in Beijing are best revealed.

Table 5 shows the eigenvalues and contribution rates of the urban thermal environment-related principal components. The first principal component has the highest contribution rate of 46.978%. The accumulated contribution rate of the first four principal components contain up to 87.909% of the information from the seven original variables. Therefore, the first four principal components can well reflect the major forming causes of the urban thermal environment in Beijing.

Table 5 The eigenvalues and contribution rates of the principal components of UHI in Beijing

The principal components	Eigenvalues	Contribution rates/%	Accumulated contribution rate/%
1	3.288	46.978	46.978
2	1.326	18.948	65.925
3	0.864	12.349	78.274
4	0.674	9.635	87.909
5	0.322	4.599	92.507
6	0.309	4.416	96.923
7	0.215	3.077	100.000

Table 6 shows the load information of the original seven variables contained in the principal components. The principal component with a larger coefficient contains more of the original information. In the load matrix (Table 6), for the first principal component, NDVI is its major contributing factor, but the contributions of NDBI, road density, and population density are negative. Therefore, the first principal component reveals the relieving effect of vegetation on the urban thermal environment. For the second principal component, elevation and slope are two major contributing factors, while the contribution of SHDI is negative. Therefore, the second principal component reflects the effects of topography on the spatial distribution of the urban thermal environment. For the third principal component, NDBI and SHDI are the major contributing factors. Urban land use diversity and land use patterns are related with human activity intensity to some extent. Therefore, the third principal component reflects the comprehensive influence of spatial clustering characteristics of land use types on urban thermal environment. For the fourth principal component, road density and population density are the major contributing factors, reflecting the effects of anthropogenic heat emission, which is a major source of the urban thermal environment. Considering the contributing factors of each principal component, the factors that affect the spatial pattern of the urban thermal environment in Beijing can be ranked in the following order: vegetation coverage, topography, construction scale on the underlying surface, and anthropogenic heat emission. Comparing the contribution rates of the principal components on the urban thermal environment, the spatial distribution of vegetation most affects the overall pattern of the urban thermal environment, followed by topography, which also changes the spatial distribution. Construction scale on the underlying surface and anthropogenic heat emission enhance UHIE to some extent.

Table 6 The load matrix of principal components

The influence factors	The first principal components	The second principal components	The third principal components	The fourth principal components	The fifth principal components	The sixth principal components	The seventh principal components
Elevation	0.706	0.509	0.174	0.198	-0.033	-0.415	0.001
Slope	0.667	0.524	0.313	0.176	0.188	0.327	-0.095
NDBI	-0.721	0.346	0.486	-0.175	-0.015	0.021	0.305
Road density	-0.782	0.026	-0.21	0.439	0.377	-0.082	0.054
Population density	-0.727	0.384	-0.103	0.408	-0.362	0.095	-0.085
NDVI	0.824	-0.123	-0.325	0.274	-0.093	0.116	0.321
Shannon's diversity index	0.082	-0.714	0.583	0.374	-0.058	-0.017	-0.020

5.3 Spatial regionalization of the urban thermal environment

The proportions of land use types and the elevation difference somehow affect the analysis of the urban thermal environment among the major functional zones. Therefore, we should be able to reveal the details of regional urban thermal environment characteristics, highlight local climate characteristics, and establish better regulation measures in study on the spatial r egionalization of the urban thermal environment. In this paper, SOM is used to investigate the spatial regionalization of the urban thermal environment in Beijing.

Based on the principle of SOM spatial clustering, LST and the major PCA factors were inputted into SOM as an input layer for learning and training, and then spatial simulation was c onducted to obtain the spatial clustering results.

The input layer contains n neurons corresponding to n spatial variables, namely, the attribute values of spatial units $(p_1, p_2, \cdots, p_n)$. The attribute values of each pixel include LST (p_1), vegetation coverage (p_2), topography (p_3), underlying surface construction scale (p_4), and anthropogenic heat emission (p_5) obtained from PCA, with the proximity index (p_6) of each p ixel.

As the dominant variable, p_1 indicates the LST in each pixel. $p_2 - p_5$ are the major variables in spatial regionalization of the urban thermal environment in Beijing through the PCA method. These variables maintain the integrity in spatial regionalization of the urban thermal environment and ensure that vegetation, terrains, underlying surface construction scale, and anthropogenic heat emission are spatially consistent in each zone.

The parameter p_6 is a proximity index. To maintain the c ontinuity of boundary among zones, the proximity index is used to correct the broken spatial units. These broken spatial units are due to the output values that depend not only on its own state for each pixel but also on the state of the surrounding pixels (Tian, et al., 2003).

We suppose that the state of a pixel is $S^t\{x,y\}$ and its proximity index is $N^t_{i,j}\{x,y\}$ at a certain time, expressed as b ellow.

$$N^t_{i,j}\{x,y\} = \varphi\left(S^t_{i,j}, S^t_{i,j+1}, S^t_{i,j-1}, S^t_{i+1,j}, S^t_{i-1,j}\right) \quad (8)$$

The proximity index can be calculated from the LST level of p_1. The proximity index of each pixel is the most frequent v alue among its own LST level and the LST levels of the s urrounding pixels.

Through SOM spatial clustering simulation, the raster data of the urban thermal environment zones are transformed to vector boundary. To ensure regionalization integrity, the units with less than three pixels are not shown (Fig. 2).

Fig. 2 Regionalization of the urban thermal environment in Beijing

Table 7 Characteristics of urban thermal environment regionalization in Beijing

Grade 1	Grade 2	LST/℃	Elevation/m	NDVI	NDBI	Population density/(persons/km^2)
Ⅰ Plain	Ⅰ$_1$ Plain town high-temperature zone	36.07	47.24	0.49	-0.10	11389.10
	Ⅰ$_2$ Plain urban-rural transitional high-temperature zone	34.01	51.66	0.61	-0.18	1455.04
	Ⅰ$_3$ Plain-cropland transitional medium-temperature zone	31.77	50.57	0.72	-0.25	667.77
Ⅱ Mountain	Ⅱ$_1$ Mountain forest medium-temperature zone	28.62	391.19	0.79	-0.24	88.61
	Ⅱ$_2$ Mountain forest low-temperature zone	26.42	695.32	0.81	-0.26	43.77
	Ⅱ$_3$ Mountain cropland medium-temperature zone	30.54	511.22	0.73	-0.28	681.82
	Ⅱ$_4$ Mountain cropland-forest-grass transitional medium-temperature zone	29.22	446.89	0.80	-0.24	105.80

To more significantly interpret the thermal environment characteristics in each zone, summer LST, elevation, NDVI, NDBI, and population density were selected for statistical analysis of the regionalization of the urban thermal environment based on the connotation of four principal components obtained from PCA (Table 7). Finally, the urban thermal environment zones were named in this paper. Meanwhile, these principal components were verified whether SOM is rational in the spatial regionalization of the urban thermal environment. The zones were named based on topographical features, land use type, and temperature subzones. Finally, Beijing was divided into plain town high-temperature zone (Ⅰ_1), plain urban-rural transitional high-temperature zone (Ⅰ_2), plain-cropland transitional medium-temperature zone (Ⅰ_3), mountain forest medium-temperature zone (Ⅱ_1), mountain forest low-temperature zone (Ⅱ_2), mountain cropland medium-temperature zone (Ⅱ_3), and mountain cropland-forest-grass transitional medium-temperature zone (Ⅱ_4). Based on the spatial regionalization of the urban thermal environment, measures and suggestions were proposed to improve the urban thermal environment in Beijing.

In general, each zone spatially extends from the center radiating outward ring by ring. The main reasons is that from the topographical perspective, Beijing has widespread plains in the southeast and mountains in the northwest. Hence, the differences in altitude and vegetation coverage will affect temperature. From the perspective of urban functional distribution, the city extends outward to the urban functional expansion zone, urban development new zone, and ecological conservation development zone, with the capital core functional zone as the center. The development positioning, targets, and tasks are different among these zones. Therefore, the contributions of economic development and population to the urban thermal environment are different.

The plain town high-temperature zone covers Dongcheng, Xicheng, Chaoyang, Haidian, Shijingshan, and Fengtai districts. These districts are featured by high building density, low vegetation coverage, and high population density (11389.10 persons/km^2), which are the key factors affecting the formation of the urban thermal environment. The contributions of buildings and population to the urban thermal environment can be further alleviated through optimizing urban functions and distribution, especially control of building intensity, traffic relief, relief of population and industry, implementation of effective green measures, increasing vegetation coverage, and building science-based ventilation corridors.

The plain urban-rural transitional high-temperature zone covers northwest Haidian and Daxing districts, as well as the central parts of Tongzhou, Shunyi, and Changping districts. The temperature in the zone is lower than that in the plain town high-temperature zone, but 2.24℃ to 7.59℃ higher than in other zones. The zone has relatively low vegetation coverage, high building density, and high population density (1455.04 persons/km^2). Along with economic development and population growth, the zone is critical for relief of population from urban core areas and for industrial agglomeration. Industrial structure and population structure in the zone should be further optimized. On one hand, population should be relieved by building more public service and living facilities and by use of public transport corridors. Other measures include development coordinated with environmental protection, actively guiding high-tech industries, development of non-pollution urban industry, and prevention of heating effect caused by high-density continuous industrial development.

The plain-cropland transitional medium-temperature zone is located in the outmost layer and covers Tongzhou, Daxing, and Shunyi districts, as well as the plain regions in Pinggu, Miyun, Huairou, Changping, and Fangshan districts. The temperature in the zone is significantly lower compared with the plain town high-temperature zone and plain urban-rural transitional high-temperature zone, but 1.23℃ to 5.35℃ higher than in mountainous areas. The population density (667.77 persons/km^2) and building density largely decrease, but vegetation coverage increases to the level in mountainous areas. The zone has the largest development potential in Beijing and undertakes the transfer of industrial, population, and urban functions. Agriculture is the pillar industry in the zone. In consequence, the zone should maintain a good ecological environment. The measures include optimizing, integrating, and improving the existing development space; actively introducing eco-friendly industries such as tourism and leisure, high-tech development, and services; and promoting the industry to scale operation and to park-centered high-quality clustered group development. In addition, the zone is adjacent to mountainous forest. As such, measures should be taken to enhance the protection and construction of ecological forest and protection of ecologically sensitive areas including forest and wetlands.

The mountainous areas are generally featured by low temperature, high vegetation coverage, low development intensity, and low population density. The mountainous areas can be divided by SOM spatial clustering into mountain forest medium-temperature zone, mountain forest low-temperature zone, mountain cropland medium-temperature zone, and mountain cropland-forest-grass transitional medium-temperature zone, which are distributed like rings. The mountainous areas are important for ensuring ecological security and water resource conservation in Beijing. In particular, large-scale high-strength industrialization and urbanization should be restricted.

The mountain forest medium-temperature zone is located in the innermost part, with an average altitude of 391.19 m, which is the lowest among the four mountainous zones. Given that the mountain forest medium-temperature zone is close to the plain areas, the zone is exposed to severe human activities, development and construction in shallow mountain areas should be strictly restricted and green construction and ecological restoration should be strengthened.

The mountain forest low-temperature zone, having the largest area among the four zones, is featured by high topography (average elevation is 695.32 m), slight human activities, vigorous vegetation growth, rich resources, and high ecological environment bearing capacity and is an important ecological barrier during urban development. To protect the ecological quality in the zone and reduce imbalance in economic development, measures should be taken to improve ecological compensation, actively promote reformation in collective ecological forest right system,

and strengthen ecological forest management responsibility.

The mountain cropland medium-temperature zone is centered around Yanqing County. Population density (681.82 persons/km^2) in this zone is the largest among the four mountainous zones, and average temperature (30.54℃) is also high. Given the intense agricultural activities and location in mountainous areas, the measures of cultivation structural optimization and land leveling should be science-based and reasonable. The zone is surrounded by mountains from three sides and by water in the other side (Guanting Reservoir in the south). Measures should be taken to prevent soil and water loss caused by sloppy farming and environmental pollution induced by unreasonable fertilization.

The mountain cropland-forest-grass transitional medium-temperature zone is located in the cropland-grassland ecotone between the mountain forest medium-temperature zones and mainly covers the middle and north parts of Huairou and Miyun counties. The temperature is higher than in the mountain cropland low-temperature zone. The zone is featured by high landscape heterogeneity, strong intersection between cropland-forest-grassland, and high ecological vulnerability. Ecological vulnerability assessment, green isolation, and protection of the surrounding ecological environment should be undertaken in a gricultural activities in ecologically vulnerable areas such as forest-grassland ecotone and reservoirs.

6 CONCLUSIONS

MODIS LST products were used to analyze the spatiotemporal diversity of LST in Beijing. Nighttime UHI in Beijing is more hierarchical, but daytime UHI is dispersed. High-temperature zones in summer are highly aggregated, radiating outward from the urban part, indicating large UHI intensity. UHI is affected by solar radiation and, to some extent, by anthropogenic factors.

In this paper, an assessment system of the urban thermal environment was built and used in PCA in Beijing. The factors that affect the spatial pattern of the urban thermal environment in Beijing can be ranked in the following order: vegetation coverage, topography, construction scale on the underlying surface, and anthropogenic heat emission. In deciding the overall distribution of LST, vegetation coverage and topography are the critical mechanisms, urban population and industrial centralization are the realizing mechanisms, and urban functional regionalization and ecological planning and design are the preventive mechanisms.

The urban thermal environment zones were named based on topographical features and subzones: plain town high-temperature zone, plain urban-rural transitional high-temperature zone, plain-cropland transitional medium-temperature zone, mountain forest medium-temperature zone, mountain forest low-temperature zone, mountain cropland medium-temperature zone, and mountain cropland-forest-grass transitional medium-temperature zone. Given the difference in the forming mechanisms of the urban thermal environment, the current development characteristics, eco-carrying capacity, and the limiting conditions among these zones, specific development strategies were proposed to improve the urban thermal environment in Beijing.

In general, through analysis of the spatiotemporal distributions in the urban thermal environment, an assessment system of the urban thermal environment was designed. Based on the differences in urban thermal environment forming mechanisms among zones, the urban thermal environment was regionalized in a scientific method. This study is significant for guiding planning and management of the urban thermal environment in cities and can help to effectively alleviate UHIE.

REFERENCES

Chen A L, Sun R H and Chen L D. 2012. Studies on urban heat island from a landscape pattern view: a review. Acta Ecologica Sinica, 32 (14): 4553 – 4565

Hao C Y, Wu S H and Li S C. 2008. Study on the method of areal differentiation based on SOFM. Advance in Earth Sciences, 27(5): 121 – 127

Jiang J and Qiao Z. 2012. Impact analysis of land surface temperature (LST) based on land use change in Beijing. Remote Sensing Information, 27(3): 105 – 111

Jiang T H, Shu J and Deng L T. 2004. Wavelet characteristics of urban heat island in Shanghai city. Journal of Tropical Meteorology, 20 (5): 515 – 522

Kidder S Q and Essenwanger O M. 1995. The effect of clouds and wind on the difference in nocturnal cooling rates between urban and rural areas. Journal of Applied Meteorology, 34 (11): 2440 – 2448 [DOI: 10.1175/1520 – 0450(1995)034 < 2440: TEOCAW > 2.0.CO;2]

Li H, Liu Q H and Zou J. 2009. Relationships of LST to NDBI and NDVI in Changsha-Zhuzhou-Xiangtan area based on MODIS data. Scientia Geographica Sinica, 29(2): 262 – 267

Lin X C, Yu S Q and Tang G L. 2005. Study on the relation between urbanization and Beijing UHI intensity. Journal of Natural Sciences, 15(7): 882 – 886

Ling Y Y and Xu J H. 2003. A nonlinear study on the urban system in Yangtze delta based on the fractal theory and the Kohonen net. Advance in Earth Sciences, 18(4): 521 – 526

Liu J Y, Liu M L, Tian H Q, Zhuang D F, Zhang Z X, Zhang W, Tang X M and Deng X Z. 2005. Spatial and temporal patterns of China's cropland during 1990—2000: an analysis based on Landsat TM data. Remote Sensing of Environment, 98(4): 442 – 456 [DOI: 10.1016/j.rse.2005.08.012]

Meng D, Gong H L and Li X J. 2010. Study on the Thermal Environment in Beijing-Tianjin-Hebei Metropolis Circle. Beijing: China Environmental Science Press

Oke T R. 1982. The energetic basis of the urban heat island. Royal Meteorological Society, 108 (455): 1 – 24 [DOI: 10.1002/qj.49710845502]

Qiao Z, Tian G J and Xiao L. 2013. Diurnal and seasonal impacts of urbanization on the urban thermal environment: A case study of Beijing using MODIS data. ISPRS Journal of Photogrammetry and Remote Sensing, 85: 93 – 101 [DOI: 10.1016/j.isprsjprs.2013.08.010]

Rao P K. 1972. Remote sensing of urban "heat islands" from an environmental satellite. Bulletin of American Meteorological Society, 53: 647 – 648

Roth M, Oke T R and Emery W J. 1989. Satellite-derived urban heat islands from three coastal cities and the utilization of such data in urban climatology. International Journal of Remote Sensing, 10(11): 1699 – 1720 [DOI: 10.1080/01431168908904002]

Schmidlin T W. 1989. The urban heat island at Toledo, Ohio. The Ohio Journal of Science, 89(3): 38 – 41

Tian G J, Liu J Y, Zhuang D F and Zhang Z X. 2003. The temporal-spatial characteristics of urban land in China in 1990s by remote sensing and GIS. Quaternary Sciences, 23(4): 421 - 427

Tian G J, Wu J G and Yang Z F. 2010. Spatial pattern of urban functions in the Beijing metropolitan region. Habitat International, 34(2): 249 - 255 [DOI: 10.1016/j.habitatint.2009.09.010]

Voogt J A and Oke T R. 2003. Thermal remote sensing of urban climates. Remote Sensing of Environment, 86(3): 370 - 384 [DOI: 10.1016/S0034 - 4257(03)00079 - 8]

Wan Z, Zhang Y, Zhang Q and Li Z L. 2004. Quality assessment and validation of the MODIS global land surface temperature. International Journal of Remote Sensing, 25(1): 261 - 274 [DOI: 10.1080/0143116031000116417]

Wang H H, Xing L X, Pan J, Qiao Z M, Li M M, Li P F and Cui C B. 2012. Research on the impact of urban landscape pattern on thermal environment using remote sensing. Environmental Protection Science, 38(4): 44 - 48

Wang K, Wan Z, Wang P, Sparrow M, Liu J and Haginoya S. 2007. Evaluation and improvement of the MODIS land surface temperature/emissivity products using ground-based measurements at a semi-desert site on the western Tibetan Plateau. International Journal of Remote Sensing, 28(11): 2549 - 2565 [DOI: 10.1080/01431160600702665]

Wang J K, Wang K C and Wang P C. 2007. Urban heat(or cool) island over Beijing from MODIS land surface temperature. Journal of Remote Sensing, 11(3): 330 - 339

Yamashita S and Sekine K. 1990. Some studies on the earth's surface conditions relating to the urban heat island. Energy and Buildings, 15(1 - 2): 279 - 288 [DOI: 10.1016/0378 - 7788(90)90140 - E]

Yang X H, Liu Y S, Jiang D, Luo C and Huang Y H. 2006. An enhanced method for spatial distributing census data: Re-classifying of rural residential. Progress in Geography, 25(3): 62 - 69

Yu M. 2011. Study on Synthetic Geo-information Tupu for Urban Heat Environment Based on RS Images. Beijing: Surveying and Mapping Press

Yue W Z. 2008. Study on Urban Landscape Pattern and Its Thermal Environment Effect Based on Remote Sensing Image. Beijing: Science Press

Zha Y, Ni S X and Yang S. 2003. An effective approach to automatically extract urban land-use from TM imagery. Journal of Remote Sensing, 7(1): 37 - 40

Zhang J H, Meng Q W and Li X. 2011. Urban heat island variations in Beijing region in multi spatial and temporal scales. Scientia Geographica Sinica, 31(11): 1349 - 1354

Zhang Z M, He G J, Xiao R B, Wang W and Ouyang Z Y. 2007. Study of urban heat island of Beijing city based on RS and GIS. Journal of Earth Sciences and Environment, 29(1): 107 - 110

Zheng D, Ge Q S, Zhang X Q, He F N, Wu S H and Yang Q Y. 2005. Regionalization in China: retrospect and prospect. Geographical Research, 24(3): 330 - 344

北京市热环境时空分异与区划

乔治，田光进

水环境模拟国家重点实验室，北京师范大学环境学院，北京 100875

摘　要:城市热环境空间区划是采用分区管理的思路来缓解城市社会经济发展与热环境之间矛盾的技术基础。本文构建城市热环境区划模型的思路为:(1)将不同时相的 MODIS 地表温度数据产品进行正规化、分级,分析 2008 年北京城市热环境时空分布特征。(2)构建城市热环境影响因素评价体系,并通过空间主成分分析计算得到热环境影响主成分因子。(3)通过自组织映射神经网络,利用热环境影响主因子,进一步对热环境进行空间区划。结果表明,北京夜间较白天城市热岛分布层次感明显,夏季白天较其他季节高温区聚合程度高。区域下垫面组成要素直接影响热环境,北京城市热环境的主成分因子依次为植被覆盖、地形地貌、城市下垫面建设规模和人为热排放,并依此将北京划为 7 个热环境区域,根据各个分区热环境成因机制差异分别提出热环境改善和调控措施。

关键词:热环境,区划,空间主成分分析,人工神经网络,北京

中图分类号:TP79　　文献标志码:A

引用格式:乔治,田光进. 2014. 北京市热环境时空分异与区划. 遥感学报,18(3): 715 –734

Qiao Z and Tian G J. 2014. Spatiotemporal diversity and regionalization of the urban thermal environment in Beijing. Journal of R emote Sensing, 1 8(3): 715 –734　[DOI: 10. 11834/jrs. 20143030]

1　引　言

城市发展往往引起城市下垫面和大气特征的剧烈变化,地表反照率、温度、湿度和空气动力学特性的变化会引起一系列微尺度和中尺度的气候变化(Roth 等,1989)。城市热岛 UHI 是城区温度高于郊区的现象(Oke,1982),是城市发展最显著的特征之一。从空间结构上看,城市热岛由各种尺度的热岛叠加而成,具有多时间、多中心的尺度结构(江田汉等,2004);从时间变化上看,热岛强度昼夜、季节变化明显,在白天和暖季中最大(Schmidlin,1989);从影响热岛的因素来看,热岛强度随风速和云量的增加而降低(Kidder 和 Essenwanger,1995),随城市/人口规模的增加而增大(Yamashita 和 Sekine,1990)。随着城市化进程加快,城市热岛效应强度和影响范围不断扩大,严重影响区域气候变化、城市大气环境和居民健康。城市热岛引发的高温灾害,将带来巨大的经济损失。城市热岛环流使城郊对流增强,洪涝灾害发生频率大大增加。城市热岛使得污染物不易扩散,空气质量严重下降,将引发城市病。近年来"城市病"日益严重,夏季高温热浪、冬季城市通风条件差而导致的大范围灰霾等严重危害人类健康和生活质量。城市化进程能否科学健康发展,已成为关乎中国社会经济又好又快发展、人民生活质量提高的关键,是国家重大需求。

早期主要使用大气温度数据进行城市热岛监测和研究,即大气城市热岛 AHUI,根据其不同层次可分为城市边界层热岛 BLHI 和城市冠层热岛 CLHI。AUHI是通过固定或移动的热探测器与空气直接接触的结果来表征城市和郊区大气温度的差异,所得到的数据是离散的点数据或线性数据。由于时间上的连续性,AUHI 可以用于昼夜对比、月份对比、年际对比和历史对比。Rao(1972)提出用热红外遥感进行城市热岛研究,标志着城市热岛研究进入新的阶段,即通过热红外遥感数据所反演的温度作为地表温度来表征地表城市热岛 SUHI (Voogt

收稿日期:2013-02-05;修订日期:2013-11-05;优先数字出版日期:2013-11-12

基金项目:国家自然科学基金(编号:41071357);国家"十二五"科技支撑计划项目(编号:2012BAC13B01)

第一作者简介:乔治(1986—),男,博士研究生,研究方向为地理信息系统应用和环境遥感。E-mail: george@ mail. bnu. edu. cn

通信作者简介:田光进(1970—),男,博士,副教授。主要从事城镇动态模型、环境遥感、地理信息系统及土地利用等方面的研究。E-mail: tianguangjin@ bnu. edu. cn

和 Oke,2003;陈爱莲 等,2012)。热红外遥感数据能够大面积覆盖地表,具有较高的空间分辨率和空间的连续性。随着遥感技术的发展,热红外遥感数据在时间分辨率上也有较大提高。已有的研究成果证明,热红外遥感反演的地表温度除了具有更高的时空分异性,其与土地利用类型的相关性更高,而城市热岛强度也比 AHUI 高,对地表特征和人类活动更为敏感(Roth 等,1989;Voogt 和 Oke,2003)。

区划研究,是探讨区域单元的形成过程、时空分异特征、调控措施,实现区域发展方案效益最大化的必要手段(郑度 等,2005)。随着城市人口持续增加和快速城市化发展,不合理的城市规划会进一步加剧城市热环境,而紧凑城市和高密度城市等不可避免的发展趋势对城市环境的要求更高。目前,通过区划研究对城市热环境识别和改善的工作相对滞后,而且同样天气条件下,城市热环境因地而异,城市热环境与城市规模和布局、人口密度、建筑密度、植被覆盖、土地用途以及城市下垫面性质有关,因此一个城市的区划方案很难完全照搬到另一个城市。正确理解城市下垫面不同要素与热环境的关系是进一步深化城市热环境研究的关键,甚至不同季相、昼夜各下垫面类型对区域热环境的贡献都有所变化(Qiao 等,2013)。本文的主旨是,通过分析城市热环境驱动因子,探索城市热岛效应形成机制,建立城市热环境分区方案,指导城市各区域针对引发城市热环境的主因子进行重点调控和防治,将热环境改善技术纳入城市规划,从而减缓或控制热岛效应。本文以 MODIS 地表温度产品为主要数据源,对北京地表温度进行时空格局分析,并进一步建立北京市热环境影响因素评价指标体系,最终通过空间主成分分析 SPCA 和自组织映射神经网络 SOM,进行北京热环境区划研究,为城市总体规划和城市生态风险评价提供决策支持。

2 研究区概况

北京市位于华北平原北部,北部是燕山山脉,西部是太行山脉,东南部是华北平原,地势西北高、东南低。北京属于典型的温带大陆性季风气候,四季分明,夏季炎热多雨,冬季寒冷干燥,春秋短促,年平均气温为 10—12℃,年平均降水量为 600—700 mm。近 50 年来北京城市人口增加 6.5 倍,基本建设投资增加近 390 倍,房屋增加 40 倍(张佳华 等,2011)。北京城市规模不断扩大,城市化水平不断提高,深刻影响着城市热环境。研究表明,北京城市房屋竣工面积每增加 10^6 m^2,北京城市热岛强度增加 0.043℃;城市基本建设投资总额每增加 100 亿元,城市热岛强度增加 0.16℃;NDVI 每升高 0.1,地表温度降低 1.6℃(林学椿 等,2005)。

3 数据来源

本文地表温度数据是由美国宇航局 NASA 提供的搭载在 Terra 卫星上的 MODIS 地表温度 8 天合成产品(MOD11)。Terra 星在上午 10:30 左右和晚上 22:30 左右过境,分别处于地表升温和降温过程。MODIS 地表温度产品是用分裂窗算法由 MODIS 的第 31 通道(10.780—11.280 μm)和第 32 通道(11.770—12.270 μm)地表比辐射率和亮温作为输入条件反演得到的,空间分辨率为 1 km。大量研究表明,MODIS 分裂窗算法反演得到的地表温度达到了 1 K 的精度(Wan 等, 2004;Wang 等,2007;王建凯等,2007)。为计算北京植被归一化指数 NDVI 和建筑归一化指数 NDBI,选用了 2008 年 MODIS 地表反射率产品(MOD09),其分辨率为 5 00 m,包含 MODIS 的第 1—7 波段数据。

其他数据包括:(1)2008 年 Landsat TM 影像数据解译的北京土地利用现状图,土地利用类型划分为耕地,林地,草地,水域,城乡、工矿、居民用地,未利用土地等 6 个 1 级土地利用类型,其中城乡、工矿、居民用地包括城镇用地、农村居民点用地和工交建设用地等 3 个 2 级土地利用类型(Liu 等,2005),来源于中国科学院资源环境科学数据中心;(2)北京数字高程数据 DEM;(3)北京市 1∶1 万数字城市数据,该数据集包括行政边界、水体、公园、铁路、公路和街区的矢量边界数据(Tian 等,2010)。

4 研究方法

4.1 MODIS 地表温度数据处理

首先利用 MODIS 数据几何纠正及重采样工具 MRT 对地表温度产品(MOD11)进行几何纠正的批处理,并利用北京行政区划进行掩膜、重采样后像元大小为 1000 m × 1000 m。查找数据头文件可得到数据产品的辐射缩放比为 0.02,辐射缩放截距为 0。因此通过式(1)计算地表温度,得到北京地表温度数据。

$$T_s = DN \times 0.02 - 273.15 \quad (1)$$

式中,T_s 为地表温度值(℃),DN 为像元灰度值。由于 MOD11 地表温度产品在有云的区域 DN 值为 0,这些区域进行波段运算后温度值均为 -273.15℃,因此需要进行云掩膜,从而去除温度的离群值。

4.2 地表温度时空分布特征

为避免云的影响,分别选取质量较好的 2008 年 4 月 22 日、7 月 19 日、10 月 7 日和 12 月 2 日(1 月市区云量太大)作为春、夏、秋、冬 4 个季节的地表温度特征。为反映不同季相的地表温度空间分布特征,将地表温度正规化,并采用密度分割技术,对城市热环境进行分级(蒋晶和乔治,2012)。首先对不同时相的地表温度进行正规化处理,使地表温度分布范围统一到 0—1。

$$T_{ni} = \frac{T_{si} - T_{\mathrm{smin}}}{T_{\mathrm{smax}} - T_{\mathrm{smin}}} \tag{2}$$

式中,T_{ni} 表示第 i 个像元正规化后的值,T_{si} 为第 i 个像元的地表温度,T_{smax} 表示北京地表温度的最大值,T_{smin} 表示北京地表温度的最小值。

利用密度分割技术对正规化后的地表温度进行等级划分,将地表温度平均划分为 7 个热力等级,分别为低温、较低温、次中温、中温、次高温、高温和特高温(表 1),制成北京地表温度等级分布图,并统计各区的面积。本文利用聚合度指数 AI 来表征北京地表温度等级的时空分异规律。聚合度指数基于同类型斑块像元间公共边界长度来计算。当类型中所有像元间存在的公共边界达到最大值时,具有最大的聚合度指数,说明该类型像元聚合度最好,分布最集中。

表 1 地表温度等级区间划分标准

地表温度等级	温度范围
低温	$T_{ni} < T_{\mathrm{mean}} - 2.5s$
较低温	$T_{\mathrm{mean}} - 2.5s \leqslant T_{ni} < T_{\mathrm{mean}} - 1.5s$
次中温	$T_{\mathrm{mean}} - 1.5s \leqslant T_{ni} < T_{\mathrm{mean}} - 0.5s$
中温	$T_{\mathrm{mean}} - 0.5s \leqslant T_{ni} < T_{\mathrm{mean}} + 0.5s$
次高温	$T_{\mathrm{mean}} + 0.5s \leqslant T_{ni} < T_{\mathrm{mean}} + 1.5s$
高温	$T_{\mathrm{mean}} + 1.5s \leqslant T_{ni} < T_{\mathrm{mean}} + 2.5s$
特高温	$T_{ni} \geqslant T_{\mathrm{mean}} + 2.5s$

注:T_{ni} 为正规化后的像元值,T_{mean} 为正规化后所有像元平均值,s 为标准差。

4.3 城市热环境影响因素评价指标体系

城市热环境的形成与演变直接关系到城市生态环境质量和可持续发展能力(岳文泽,2008)。城市作为一个复合巨系统,城市下垫面热惯量、热容量、热传导和热辐射的差异,人类活动强度不同,以及不同景观类型分布及内部结构差异等因素共同作用于城市热环境。结合遥感技术和调查资料,建立城市热环境指标体系,对城市热环境进行多变量综合分析,从而揭示城市热环境的成因机制。

岳文泽(2008)、孟丹等人(2010)以及余明(2011)分别对上海市、京津冀都市圈、闽东南城市群建立热环境影响因素评价指标体系。引发城市热岛有两大因素:一是城区土地利用和覆盖不同于郊区,二是城区人为释放的交通生产生活的废气废热远高于郊区(陈爱莲 等,2012)。纵观城市发展过程,城市热岛效应日益明显,主要体现在促进城市热岛效应增加的因素被加强,利于减少城市热岛效应的因素被削弱。因此在进行城市热环境影响因素评价时,应结合土地利用及其所承载的人为热排放,突出其对局地气候的影响,从而提出针对性更强的热环境调控措施。本文结合北京社会—经济—自然状况,构建北京热环境影响因素评价指标体系(表 2)。

表 2 北京热环境影响因素评价指标体系

	一级指标		
	城市下垫面特征	人类活动强度特征	生态环境特征
二级指标	归一化建筑指数	道路密度	高程
	景观多样性指数	人口密度	坡度
			NDVI

北京热环境影响因素评价指标体系分为两级,第一级包括城市下垫面特征、人类活动强度特征以及生态环境特征 3 个方面,每个一级指标又分别对应其二级指标。其中,人类活动强度包括生产和生活人为释放热量,但是难以直接通过遥感数据进行量化。本文通过道路密度和人口密度作为人为释放热量(汽车尾气、制冷供暖热排放等)的反映指标。二级指标的内涵及计算方法分别介绍如下。

归一化建筑指数 NDBI 可以较为准确地反映建筑用地信息。数值越大,表明建筑用地比例越高,建筑密度越高(查勇 等,2003)。本文使用 NDBI 来表征城市非渗透表面的空间分布。

$$\mathrm{NDBI} = \frac{Q_{\mathrm{SWIR}} - Q_{\mathrm{NIR}}}{Q_{\mathrm{SWIR}} + Q_{\mathrm{NIR}}} \tag{3}$$

式中,NDBI 为归一化建筑指数,Q_{SWIR} 为短波红外波段灰度值,Q_{NIR} 为近红外波段。对于 MODIS 地表反射率产品(MOD09),NIR 为第 2 波段,SWIR 为第 6

波段。历华等人(2009)利用 MODIS 数据计算长株潭地区 NDBI,范围为 -0.411—0.061,4 个季节变化范围非常接近,说明 NDBI 不会随季节发生太大变化。

景观多样性指数 SHDI,是基于信息论基础上对景观格局的丰富程度和复杂程度的综合反映(岳文泽,2008)。城市地表温度不仅与下垫面的景观类型密切联系,还与景观类型的空间组合格局相关。城市下垫面的多样性指数对城市温度的景观异质性具有明显的二次抛物线相关关系(王红红 等,2012)。计算公式为

$$\mathrm{SHDI} = -\sum_{i=1}^{m}(P_i \times \ln P_i) \tag{4}$$

式中,SHDI 为景观多样性指数,P_i 为土地利用类型 i 所占的面积比例,m 为土地利用类型的数目。将土地利用现状图与研究区 1 km × 1 km 的网格进行叠加,统计出每个网格中不同土地利用类型所占比例,并进一步计算得到多样性指数。

道路密度,以道路等级为衡量标准,按照不同的道路等级分配不同的权重,利用 Arc/Info 软件中的线密度函数实现道路密度的计算(岳文泽,2008)。公式为

$$R_{\mathrm{d}} = \frac{((L_1 \times W_1) + (L_2 \times W_2) + \cdots + (L_n \times W_n))}{Area} \tag{5}$$

式中,R_{d} 为道路密度,L_n 为研究区 1 km × 1 km 单元格内的道路长度,W_n 为道路权重,$Area$ 为单元格面积。

人口密度,是指一定时期某地区人口数与该地区面积之比,反映人口在地域分布的稠密程度。本研究采用由中国科学院资源环境科学数据中心提供的 1 km 人口空间统计数据。该数据是利用人口(统计)数据空间化技术,选取对人口空间分布影响最直接的城镇居民地、农村居民地和耕地因子,结合人口统计数据,以乡镇为样本,构建人口数据空间化模型(杨小唤 等,2006)。

高程和坡度。已有研究证实,温度与高程、坡度呈反比关系,高程越低、坡度越小,越有利于热岛中心的形成(张兆明 等,2007)。本文用北京行政区的数字高程模型进行掩膜,并利用 Arc/Info 软件进一步计算北京坡度数据。

NDVI 是反映绿色植被的相对丰度和活性的辐射量值,指示了城乡地表性质的差异(蒸发量和热容量)。但是冬季 NDVI 不能很好地反映地表性质,因为北京多为落叶植被,冬季光合作用活动弱。

$$\mathrm{NDVI} = \frac{Q_{\mathrm{NIR}} - Q_{\mathrm{Red}}}{Q_{\mathrm{NIR}} + Q_{\mathrm{Red}}} \tag{6}$$

式中,NDVI 为归一化植被指数,Q_{NIR} 为近红外波段灰度值,Q_{Red} 为红色波段灰度值。对于 MODIS 地表反射率产品(MOD09),NIR 为第 2 波段,Red 为第 1 波段。

由于影响因子的分级或计量单位不同,对城市热环境的影响不具有可比性,必须进行指标量化处理。本研究采用极差标准化方法,对各因子进行标准化处理。

$$X_i' = \frac{X_i - X_{\min}}{X_{\max} - X_{\min}} \tag{7}$$

式中,X_i' 为影响因子经过标准化后的值,X_i 为影响因子的实际值;$X_{\min}$ 为影响因子在研究区域内的最小值,$X_{\max}$ 为影响因子在研究区域内的最大值。经过标准化处理后,消除了影响因子取值范围和量纲的影响。

4.4 城市热环境影响因素空间主成分分析

城市热环境受到诸多因子的综合影响,并且影响因子之间也存在着一定的相关性,直接进行多准则判断存在问题(岳文泽,2008)。通过空间主成分分析方法,利用正交旋转变换来消除影响因子的相关性或冗余度,可以明确各主成分的物理含义,同时也避免了多准则判断权重不合理的弊端,从而进一步揭示城市热环境的内在机制。

本文在 Arc/Info 软件 GRID 模块支持下,采用空间变量的主成分分析方法,实现对影响城市热环境形成的空间变量主成分分析。通过北京城市热环境目标信息空间因子主成分分析特征值和贡献率的计算,从而选取主成分,并明确各个主成分对于城市热环境形成的物理意义,进一步深化对城市热岛形成的机制研究。

4.5 基于自组织映射神经网络的热环境区划

自组织映射(SOM)神经网络模型通过寻找最优权值矢量对输入变量进行非监督聚类。该方法可以避免由于人工确定各指标或各层次权重所带来的主观性。SOM 模型也越来越多地应用在城市系统的模拟研究中(凌怡莹和徐建华,2003;岳文泽,2008;郝成元 等,2008)。本文将 GIS 与 SOM 在空间上进行结合,模拟空间样本的竞争,从而进行空间聚类,不仅提高了 SOM 模型的应用能力,而且对城市热环境规划分区提供了新的方法。

SOM 网络是由输入层和竞争层构成的两层网络,输入层用于接收输入模式,输出层神经元按照 2 维阵列排列,两层之间各神经元实现双向互连接,SOM 网络通过寻找最优权值矢量对输入模式集合进行聚类模拟(凌怡莹和徐建华,2003)。

网络的输入模式为

$$\boldsymbol{P}_k = (p_1^k, p_2^k, \cdots, p_N^k), k = 1, 2, \cdots, q$$

竞争层神经元矢量为

$$\boldsymbol{A}_j = (a_{j1}, a_{j2}, \cdots, a_{jM}), j = 1, 2, \cdots, M$$

式中,$\boldsymbol{P}_k$ 为连续值,$\boldsymbol{A}_j$ 为数字量,q 为学习模式个数,N 为输入层神经元个数,M 为竞争层神经元个数。竞争层神经元 j 与输入层神经元之间的连接权值矢量为

$$\boldsymbol{W}_j = (w_{j1}, w_{j2}, \cdots, w_{jN}), j = 1, 2, \cdots, M$$

本文将空间主成分分析得到的主导因子作为输入变量导入 SOM 网络中,在 Matlab 软件和 GIS 技术的支持下,对城市热环境成因机制进行空间聚类,揭示北京热环境成因机制的空间差异,概括成因机制的主要类型,从而进行北京热环境分区,并针对分区方案提出缓解城市热岛的措施。

5 北京城市热环境结果分析

5.1 城市热环境时空分布特征分析

对各温度等级区域分析,中温区所占比重最大。根据温度等级的涵义,中温区可以视为某一时间内北京地表温度的“平均值”,通过对“低温区”(低温、较低温和次中温)和“高温区”(次高温、高温和特高温)的距平分析,可以更直观地得到北京地表温度分布的时空分异(图 1 和表 3)。

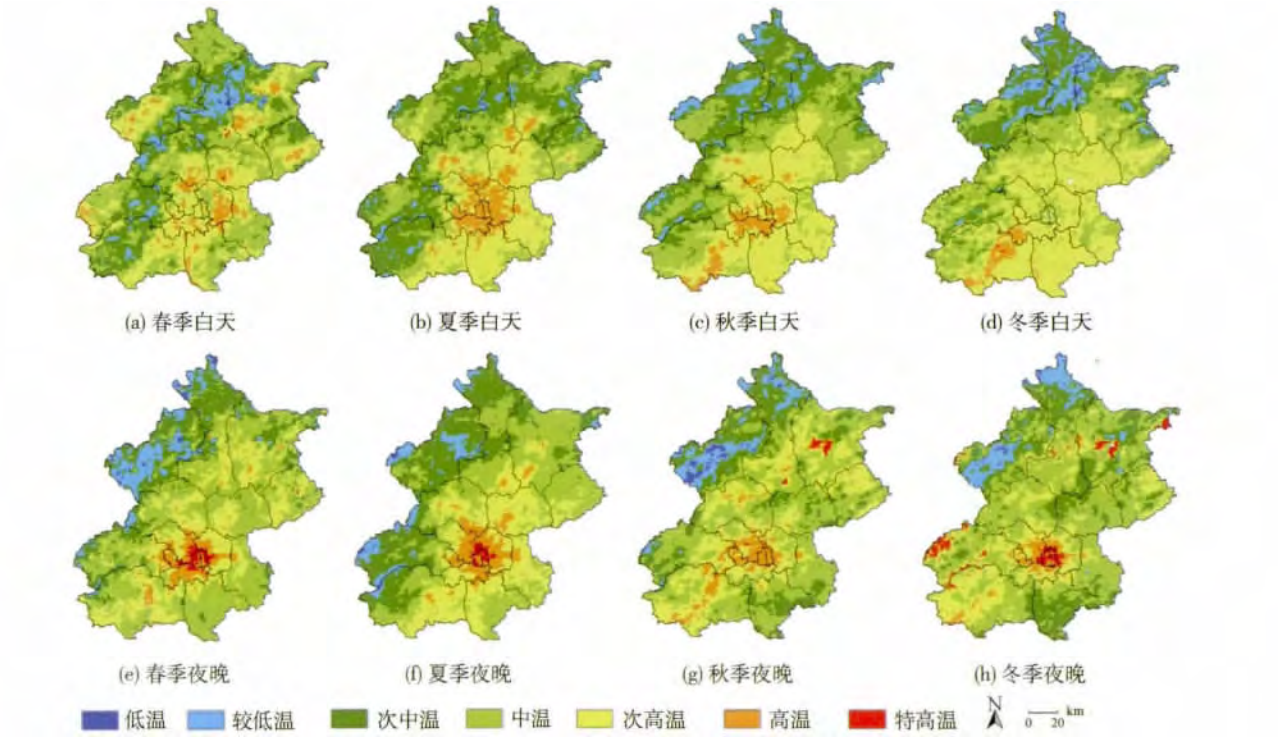

图 1 北京 2008 年地表温度等级分布

表 3 北京 2008 年地表温度热力等级比例 /%

等级	白天				夜晚			
	春季	夏季	秋季	冬季	春季	夏季	秋季	冬季
低温	0.24	0.01	0.01	0.79	0.62	0.29	1.23	0.38
较低温	6.92	3.80	7.45	8.70	7.97	5.64	6.07	5.71
次中温	24.54	34.22	25.80	20.03	18.01	26.61	20.13	22.55
中温	34.79	27.95	29.83	30.42	42.58	34.68	41.16	44.28
次高温	27.07	25.60	31.25	37.21	24.55	25.47	24.93	20.00
高温	6.34	8.42	5.66	2.81	5.29	6.59	6.03	5.08
特高温	0.10	0.00	0.00	0.04	0.99	0.72	0.45	2.00

分析昼夜温度等级分布,夜间中温区所占比重远大于白天,“低温区”和“高温区”所占比重小于白天,说明北京夜间温度较白天各地区差异小。从空间格局分析,夜间各温度等级的 AI 值也高于白天,夜间城市热岛分布具有明显的空间层次感,即从城中心的高值区域,经过城郊的次高值区域,再到城市外围低值区域。这是由于城乡地表吸收和存储热量性能存在差异,城区下垫面对太阳辐射反射率小,热容量大,导热率高,所以存储的热量高;另外,地面长波辐射经过建筑物和地面间多次反射向大气中散发的热量较少。但是值得注意的是,夜间较白天相比,特高温区分布有两处较明显,一处集中在城区,并且春、夏、冬季较为明显,而秋季不明显,这与城区人类活动强度大,集中供热和制冷散热有很大关系;另一处集中在密云水库等大面积水体,这与水体比热大,当同样受冷受热时温度变化小有关。

分析季节温度变化,夏季白天中温区所占比重最少,“高温区”所占比重也最少,但是“低温区”所占比重最大,而冬季白天恰恰相反。从 AI 来看,夏季白天“高温区”最高,以城区为中心,向外辐射,从而显示了较大的城市热岛强度(表 4)。白天内陆城市温度与土地利用类型有较强的相关性,工业用地温度最高,而植被和河流温度最低。由于 Terra 星是上午 10:30 过境,正处于地表升温阶段,北京远郊区多为山地,海拔较平原区高,再加上茂密的植被覆盖,夏季温度远低于城区,但是北京植被多为落叶植被,冬季植被干枯,地表裸露,土壤冻结,辐射冷却更强,所以温度差异较夏季小,“低温区”不明显。同时冬季白天“高温区”AI 也较低,分布比较零散,说明受人类活动影响程度大。尤其在房山区中北部地区高能耗的工业企业地区,出现了大面积的高温区。另外冬季白天,北京市出现了“城市冷岛”现象。

表 4 北京 2008 年地表温度热力等级聚合度指数

等级	白天				夜晚			
	春季	夏季	秋季	冬季	春季	夏季	秋季	冬季
低温	58.46	N/A	N/A	45.15	54.10	57.32	66.76	46.36
较低温	71.95	60.72	68.63	68.15	71.15	75.10	72.69	78.04
次中温	73.36	83.39	79.75	73.09	71.70	86.67	75.16	75.19
中温	74.04	77.31	82.02	72.97	80.48	84.25	81.15	80.04
次高温	76.81	84.16	89.20	83.86	75.36	83.85	78.10	72.13
高温	66.96	81.27	78.97	73.32	72.21	83.14	74.91	62.89
特高温	37.50	0.00	0.00	57.14	71.81	78.50	76.92	68.40

5.2 城市热环境影响因素主成分分析

通过以上分析可知,夏季白天,北京市高温区与低温区差异明显且分布集中,热岛影响范围大。夏季植被茂密,对城市温度影响较冬季大。白天人类活动强度也较夜间大。因此本文选择影响北京市热环境表征最典型的夏季白天地表温度相关的各因子做主成分分析,从而更好地得到各因子对北京市热环境的影响关系。

表 5 显示了北京城市热环境目标信息空间因子主成分的特征值和贡献率。从表 5 中可见,第一主成分的贡献率最大,达到 46.978%。从累积贡献率来看,前 4 个主成分的累积贡献率已经包含了原始 7 个变量中高达 87.909% 的信息,由此认为前 4 个主成分已经能够较好地反映北京城市热环境形成的主要原因。

表 5 主成分的特征值及其贡献率

主成分	特征值	贡献率/%	累积贡献率/%
1	3.288	46.978	46.978
2	1.326	18.948	65.925
3	0.864	12.349	78.274
4	0.674	9.635	87.909
5	0.322	4.599	92.507
6	0.309	4.416	96.923
7	0.215	3.077	100.000

表 6 显示了经过主成分变换后,北京城市热环境成因的每一个主成分包含原 7 个变量的信息载荷

情况。主成分所对应的系数越大,包含原变量信息成分越高。根据主成分载荷矩阵,对于第 1 主成分而言,归一化植被指数为该主成分的主要贡献因子,而从表 6 中可以明显看出,归一化建筑指数,道路密度和人口密度对第 1 主成分的贡献为负。第 1 主成分揭示了植被对城市热环境的缓解作用;对于第 2 主成分,高程和坡度占了较大比重,对其有明显的正贡献,而景观多样性指数则对该主成分产生了负影响。第 2 主成分反映地形影响城市热环境的空间分布格局;对于第 3 主成分,归一化建筑指数和景观多样性指数为其主要贡献因子。城市土地利用多样性与土地利用格局以及人类活动强度具有一定的对应关系。第 3 主成分可以揭示土地利用类型空间集聚特征对城市热环境的综合影响。对于第 4 主成分,道路密度和人口密度为主要贡献因子。第 4 主成分反映了人的热量排放也是城市热环境的主要热源之一,对城市热岛效应具有明显的加强作用。综合考虑各个主成分的主要贡献因子,影响北京城市热环境空间格局的因子按照作用度大小,可以概括为植被覆盖、地形地貌、城市下垫面建设规模和人为热排放 4 个主因子。从所选主成分对城市热环境的贡献率来看,植被覆盖的空间分布最能影响城市热环境的总体格局,其次地形地貌因素也改变了城市热环境的空间分布,而城市下垫面建设规模和人为热排放则在一定程度上加大了城市热岛的强度。

表 6 主成分载荷矩阵

热环境影响因子	第 1 主成分	第 2 主成分	第 3 主成分	第 4 主成分	第 5 主成分	第 6 主成分	第 7 主成分
高程	0.706	0.509	0.174	0.198	−0.033	−0.415	0.001
坡度	0.667	0.524	0.313	0.176	0.188	0.327	−0.095
NDBI	−0.721	0.346	0.486	−0.175	−0.015	0.021	0.305
道路密度	−0.782	0.026	−0.21	0.439	0.377	−0.082	0.054
人口密度	−0.727	0.384	−0.103	0.408	−0.362	0.095	−0.085
NDVI	0.824	−0.123	−0.325	0.274	−0.093	0.116	0.321
SHDI	0.082	−0.714	0.583	0.374	−0.058	−0.017	−0.020

5.3 城市热环境空间区划

不同主体功能区中土地利用类型所占比例、高程差异在一定程度上影响了城市热环境分析,因此,在进行城市热环境空间区划研究中,应该更细致地反映区域热环境特征,突出局地气候特征,并制定更完善的调控措施。本文利用 SOM 神经网络进行北京市热环境空间区划探讨。

根据 SOM 空间聚类原理,将地表温度和 PCA 分析得到的主因子作为 SOM 网络输入层,输入 SOM 网络进行学习训练,然后进行空间模拟,最终得到空间聚类结果。

输入层有 n 个神经元对应的 n 个空间变量(p_1, p_2,…,p_n),即空间单元的属性值。每个空间单元的属性值包括:地表温度 p_1;由主成分分析得到的植被覆盖 p_2,地形地貌 p_3,城市下垫面建设规模 p_4 和人为热排放 p_5 4 个主因子;每个单元的邻近性指数 p_6。

变量 p_1 是每个空间单元的地表温度值。在北京城市热环境空间区划中作为主导变量。变量 p_2—p_5 分别是由主成分分析得到的主因子,是为保持热环境空间区划的完整性,在每一个区划内确保植被覆盖、地形地貌、城市下垫面建设规模和人为热排放具有较高的空间一致性。

变量 p_6 是邻近性指数。为了保持区划边界的连续性,采用邻近性指数来纠正细碎的空间单元,因为每个空间单元的输出值不仅取决于自身的状态,还取决于其周围空间单元的状态值(田光进 等,2003)。

设某一时刻,每个空间单元的自身状态为 $S^t\{x,y\}$,其邻近性指数为 $N^t_{i,j}\{x,y\}$。

$$N^t_{i,j}\{x,y\} = \varphi\left(S^t_{i,j},S^t_{i,j+1},S^t_{i,j-1},S^t_{i+1,j},S^t_{i-1,j}\right) \quad (8)$$

式中,函数 φ 用于计算每个空间单元邻近性指数。邻近性指数由变量 p_1 的热力等级求出,每个空间单元的邻近性指数即为该空间单元本身热力等级的值与周围空间单元热力等级出现频率最高的值。

通过 SOM 空间聚类模拟,将得到的北京城市热环境区划栅格数据转为完整的边界矢量曲线(为保证区划完整性,不满 3 个像元的图斑忽略不计)(图 2)。

为更直观地表示各区划的热环境特征,根据主成分分析得到的 4 个主因子涵义,本文选择夏季地表温度和高程、NDVI、NDBI 和人口密度等热环境影响因子(表 7),对各区划热环境特征进行统计分析,最终进行热环境区划命名。同时也进一步检验了通过主成分分析因子进行 SOM 热环境空间区划结果的合理性。命名由地貌特征、土地利用类型和温度区分级 3 个部分组成,最终将北京划为平原城镇高温区 $Ⅰ_1$、平原城乡过渡高温区 $Ⅰ_2$、平原农耕过渡中温区 $Ⅰ_3$、山地森林中温区 $Ⅱ_1$、山地森林低温区 $Ⅱ_2$、山地耕地中温区 $Ⅱ_3$ 和山地耕—林—草过渡中温区 $Ⅱ_4$。针对北京城市热环境区划结果(图 2),提出改善北京城市热环境的措施与建议。

图 2 北京热环境区划

表 7 北京热环境区划特征统计

一级分区	二级分区	地表温度/℃	高程/m	NDVI	NDBI	人口密度/(人/km^2)
Ⅰ平原区	$Ⅰ_1$ 城镇高温区	36.07	47.24	0.49	−0.10	11389.10
	$Ⅰ_2$ 城乡过渡高温区	34.01	51.66	0.61	−0.18	1455.04
	$Ⅰ_3$ 农耕过渡中温区	31.77	50.57	0.72	−0.25	667.77
Ⅱ山区	$Ⅱ_1$ 森林中温区	28.62	391.19	0.79	−0.24	88.61
	$Ⅱ_2$ 森林低温区	26.42	695.32	0.81	−0.26	43.77
	$Ⅱ_3$ 耕地中温区	30.54	511.22	0.73	−0.28	681.82
	$Ⅱ_4$ 耕—林—草过渡中温区	29.22	446.89	0.80	−0.24	105.80

总体来看,各分区由中心区向外层层扩展。分析原因如下:(1)从地形来看,北京东南部为平原区,西北部为山区,海拔高度和植被覆盖的差异对温度有所影响;(2)从城市功能布局来看,以首都核心功能区为中心,到外围的城市功能拓展区、城市发展新区和生态涵养发展区,各区域发展定位、发展目标和发展任务不同,其经济发展、人口对热环境的贡献也有所差异。

平原城镇高温区主要包括东城区、西城区、朝阳区、石景山区、海淀区和丰台区,这些地区城市建筑密度高,植被覆盖率低,人口分布集中(11389.10 人/km^2),这些因素对城市热环境的形成起主导作用。通过优化城市功能和布局,尤其是控制建设强度、交通梳理、疏解人口与产业,实行高效的绿化措施,增加植被覆盖度,并且科学地建立通风廊道,可进一步缓解因建筑和人口因素对热环境的贡献。

平原城乡过渡高温区主要包括海淀区西北以及大兴区、通州区、顺义区和昌平区靠近中心区的部分。该区比平原城镇高温区温度稍低,但仍然明显高于其他地区 2.24—7.59℃。相比其他地区,该区仍是植被覆盖率较低,建筑密度高,人口分布密集(1455.04 人/km^2)的地区。随着经济发展和人口增长,这些地区是未来北京市重点发展的地区,将进一步承担城区人口疏解和产业集聚等重要职能。人口结构和产业结构进一步优化,是平原城乡过渡高温区发展的关键,一方面,积极改善公共服务、居住配套,综合运用公共运输廊道进行人口疏解的引导;另一方面,城市建设要充分与生态环境协调发展,积极引导无污染的高新技术产业,防止工业高密度连片发展所引起的热效应。

平原农耕过渡中温区位于平原地区最外层,包括通州、大兴、顺义,以及平谷、密云、怀柔、昌平、房山的山前平原地区。该区较平原城镇高温区、平原城乡过渡高温区温度有较大下降,但仍高于山区温

度(1.23—5.35℃)和人口密度(667.77 人/km^2),建筑密度有了大幅度下降,植被覆盖也有所增加,接近山区水平。该区作为本市开发潜力最大的地区,承接产业、人口和城市功能的转移。由于该区主要以农业生产活动为主,因此应引导生态友好型的产业,注重维持好现有生态环境。科学优化、整合、完善现有的发展空间,引入旅游休闲、高新技术研发与服务,积极推进产业向规模经营集中、工业向园区集中的高品质、组团式的集群发展模式。另外该区紧邻山区林地,要加强该区生态林地的保护和建设,有效保护湿地和森林等生态脆弱地区。

山区总体表现出温度低、植被覆盖高、开发强度低和人口密度小的特征,但通过 SOM 空间聚类,可进一步分为山地森林中温区、山地森林低温区、山地耕地中温区和山地耕—林—草过渡中温区,呈环状(带状)分布。山区对保障北京生态安全和水资源涵养具有至关重要的作用,要严格限制大规模高强度工业化、城镇化开发。

山地森林中温区位于最内层,平均高度为 391.19 m,在 4 个山区区域中,海拔最低。该区域最接近平原地区,受人类活动影响较大,因此在浅山区应严格控制开发建设,并加强绿化建设和生态恢复。

山地森林低温区作为山区中面积最大的区域,由于地势最高(平均高度为 695.32 m),受人类活动影响最小。该区域植被生长状况最好,具有较高的资源禀赋和生态环境承载能力,是城市发展的重要生态屏障。为保护该区优质生态环境,降低经济发展的不平衡性,要完善生态林补偿措施,积极推进集体生态林权制度的改革,强化生态林管护责任,这也是保障该区生态环境质量的重要手段。

山地耕地中温区是以延庆县为中心的农耕区。在山区中,山地耕地中温区为人口密度较大(681.82 人/km^2),平均温度也较高的地区(30.54℃)。由于该区农业活动强度大,又处于山区,耕地结构优化和土地平整等措施要科学合理。该区三面环山,一面环水(南部为官厅水库),防止由于坡耕地引起的水土流失以及由于不合理施肥引起的环境污染,是需要特别注意的生态环境问题。

山地耕—林—草过渡中温区是位于山地森林低温区之间的耕地—林草交错区,主要位于怀柔和密云中北部地区,温度较山地森林低温区高。山地耕—林—草过渡中温区内景观异质性大,耕地、林地和草地交错性强,生态脆弱性较高。开展生态脆弱性评价,在林草交错带、水库等生态敏感地区,积极进行绿化隔离,从事农耕活动时对周围生态环境进行保护。

6 结 论

通过 MODIS 遥感数据所提取的地表温度产品,分析了北京地表温度时空格局。北京夜间城市热岛分布层次感明显,白天较为分散;夏季高温区聚集程度高,以城市为中心,向外辐射,表现出较大的城市热岛强度。城市热岛除受到太阳辐射因素外,在一定程度上还体现人为因素的影响。

本文设计了北京热环境影响因素评价指标体系,并对其进行主成分分析。影响北京城市热环境空间格局的因子按照作用度大小,可以概括为植被覆盖、地形地貌、城市下垫面建设规模和人为热排放 4 个主因子。植被覆盖和地形是地表温度总体分布格局的决定机制,城市人口和产业集聚是其实现机制,而城市功能区划和生态规划设计是其阻推机制。

通过 SOM 对北京热环境进行区划,分为平原城镇高温区、平原城乡过渡高温区、平原农耕过渡中温区、山地森林中温区、山地森林低温区、山地耕地中温区和山地耕—林—草过渡中温区。针对北京城市热环境成因机制差异,根据不同区域的现状发展特征、生态环境承载能力和限制条件,提出改善北京城市热环境的分区域发展策略。

总之,通过城市热环境时空分布格局分析,设计热环境影响因素评价指标体系,并根据不同区域热环境成因机制差异,对城市热环境进行了科学地区划。这对城市热环境的规划管理具有积极的意义,为有效缓解城市热岛效应提供了范式参考。

参考文献(References)

陈爱莲, 孙然浩, 陈利顶. 2012. 基于景观格局的城市热岛研究进展. 生态学报, 32(14): 4553 – 4565

郝成元, 吴绍洪, 李双成. 2008. 基于 SOFM 的区域界线划分方法. 地理科学进展, 27(5): 121 – 127

蒋晶, 乔治. 2012. 北京市土地利用变化对地表温度的影响分析. 遥感信息, 27(3): 105 – 111

江田汉, 束炯, 邓莲堂. 2004. 上海城市热岛的小波特征. 热带气象学报, 20(5): 515 – 522

Kidder S Q and Essenwanger O M. 1995. The effect of clouds and wind on the difference in nocturnal cooling rates between urban and rural areas. Journal of Applied Meteorology, 34(11): 2440 – 2448 [DOI:

10.1175/1520-0450(1995)034<2440:TEOCAW>2.0.CO;2]

历华,柳钦火,邹杰. 2009. 基于MODIS数据的长株潭地区NDBI和NDVI与地表温度的关系研究. 地理科学,29(2):262-267

林学椿,于淑秋,唐国利. 2005. 北京城市化进程与热岛强度关系的研究. 自然科学进展,15(7):882-886

凌怡莹,徐建华. 2003. 基于分形理论和Kohonen网络的城镇体系的非线性研究——以长江三角洲地区为例. 地球科学进展,18(4):521-526

Liu J Y, Liu M L, Tian H Q, Zhuang D F, Zhang Z X, Zhang W, Tang X M and Deng X Z. 2005. Spatial and temporal patterns of China's cropland during 1990—2000: an analysis based on Landsat TM data. Remote Sensing of Environment, 98(4): 442-456 [DOI: 10.1016/j.rse.2005.08.012]

孟丹,宫辉力,李小娟. 2010. 京津冀都市圈热环境研究. 北京:中国环境科学出版社

Oke T R. 1982. The energetic basis of the urban heat island. Royal Meteorological Society, 108(455): 1-24 [DOI: 10.1002/qj.49710845502]

Qiao Z, Tian G J and Xiao L. 2013. Diurnal and seasonal impacts of urbanization on the urban thermal environment: A case study of Beijing using MODIS data. ISPRS Journal of Photogrammetry and Remote Sensing, 85: 93-101 [DOI: 10.1016/j.isprsjprs.2013.08.010]

Rao P K. 1972. Remote sensing of urban "heat islands" from an environmental satellite. Bulletin of American Meteorological Society, 53: 647-648

Roth M, Oke T R and Emery W J. 1989. Satellite-derived urban heat islands from three coastal cities and the utilization of such data in urban climatology. International Journal of Remote Sensing, 10(11): 1699-1720 [DOI: 10.1080/01431168908904002]

Schmidlin T W. 1989. The urban heat island at Toledo, Ohio. The Ohio Journal of Science, 89(3): 38-41

田光进,刘纪远,庄大方,张增祥. 2003. 基于遥感与GIS的20世纪90年代中国城镇用地时空特征. 第四纪研究,23(4):421-427

Tian G J, Wu J G and Yang Z F. 2010. Spatial pattern of urban functions in the Beijing metropolitan region. Habitat International, 34(2): 249-255 [DOI: 10.1016/j.habitatint.2009.09.010]

Voogt J A and Oke T R. 2003. Thermal remote sensing of urban climates. Remote Sensing of Environment, 86(3): 370-384 [DOI: 10.1016/S0034-4257(03)00079-8]

Wan Z, Zhang Y, Zhang Q and Li Z L. 2004. Quality assessment and validation of the MODIS global land surface temperature. International Journal of Remote Sensing, 25(1): 261-274 [DOI: 10.1080/0143116031000116417]

王红红,邢立新,潘军,乔振民,李淼淼,李鹏飞,崔承宝. 2012. 城市景观格局对热环境影响遥感研究. 环境保护科学,38(4):44-48

Wang K, Wan Z, Wang P, Sparrow M, Liu J and Haginoya S. 2007. Evaluation and improvement of the MODIS land surface temperature/emissivity products using ground-based measurements at a semi-desert site on the western Tibetan Plateau. International Journal of Remote Sensing, 28(11): 2549-2565 [DOI: 10.1080/01431160600702665]

王建凯,王开存,王普才. 2007. 基于MODIS地表温度产品的北京城市热岛(冷岛)强度分析. 遥感学报,11(3):330-339

Yamashita S and Sekine K. 1990. Some studies on the earth's surface conditions relating to the urban heat island. Energy and Buildings, 15(1-2): 279-288 [DOI: 10.1016/0378-7788(90)90140-F]

杨小唤,刘业森,江东,罗春,黄耀欢. 2006. 一种改进人口数据空间化的方法:农村居住地重分类. 地理科学进展,25(3):62-69

余明. 2011. 遥感影像的城市热环境综合信息图谱研究. 北京:测绘出版社

岳文泽. 2008. 基于遥感影像的城市景观格局及其热环境效应研究. 北京:科学出版社

查勇,倪绍祥,杨山. 2003. 一种利用TM图像自动提取城镇用地信息的有效方法. 遥感学报,7(1):37-40

张佳华,孟倩文,李欣. 2011. 北京城区城市热岛的多时空尺度变化. 地理科学,31(11):1349-1354

张兆明,何国金,肖荣波,王威,欧阳志云. 2007. 基于RS与GIS的北京市热岛研究. 地球科学与环境学报,29(1):107-110

郑度,葛全胜,张雪芹,何凡能,吴绍洪,杨勤业. 2005. 中国区划工作的回顾与展望. 地理研究,24(3):330-344